INTERFACE

royalsocietypublishing.org/journal/rsif

Research

Cite this article: Ross CJ *et al*. 2019 An investigation of the glycosaminoglycan contribution to biaxial mechanical behaviours of porcine atrioventricular heart valve leaflets. *J. R. Soc. Interface* **16**: 20190069.
http://dx.doi.org/10.1098/rsif.2019.0069

Received: 3 February 2019
Accepted: 3 June 2019

Subject Category:
Life Sciences–Engineering interface

Subject Areas:
bioengineering, biomechanics

Keywords:
glycosaminoglycan removal, biaxial mechanical testing, atrioventricular heart valves, leaflet microstructure, stress relaxation

Author for correspondence:
Chung-Hao Lee
e-mail: ch.lee@ou.edu

†Equal first-authored contribution.
‡Present address: National Institute of Technology Rourkela, India.

Electronic supplementary material is available online at http://dx.doi.org/10.6084/m9.figshare.c.4536953.

THE ROYAL SOCIETY PUBLISHING

An investigation of the glycosaminoglycan contribution to biaxial mechanical behaviours of porcine atrioventricular heart valve leaflets

Colton J. Ross[1], Devin W. Laurence[1,†], Jacob Richardson[1], Anju R. Babu[1,‡], Lauren E. Evans[1], Ean G. Beyer[1], Rachel C. Childers[2], Yi Wu[1], Rheal A. Towner[4], Kar-Ming Fung[5,6], Arshid Mir[7], Harold M. Burkhart[8], Gerhard A. Holzapfel[9,10] and Chung-Hao Lee[1,3]

[1]Biomechanics and Biomaterials Design Laboratory, School of Aerospace and Mechanical Engineering, [2]Stephenson School of Biomedical Engineering, and [3]Institute for Biomedical Engineering, Science and Technology, The University of Oklahoma, Norman, OK, USA
[4]Advanced Magnetic Resonance Center, MS 60, Oklahoma Medical Research Foundation, Oklahoma City, OK, USA
[5]Department of Pathology, [6]Stephenson Cancer Center, [7]Division of Pediatric Cardiology, Department of Pediatrics, and [8]Division of Cardiothoracic Surgery, Department of Surgery, The University of Oklahoma Health Sciences Center, Oklahoma City, OK, USA
[9]Institute of Biomechanics, Graz University of Technology, Graz, Austria
[10]Department of Structural Engineering, Norwegian University of Science and Technology (NTNU), Trondheim, Norway

CJR, 0000-0002-8871-6016; DWL, 0000-0002-9681-4708; ARB, 0000-0003-2259-5896; RCC, 0000-0001-9430-4897; GAH, 0000-0001-8119-5775; C-HL, 0000-0002-8019-3329

The atrioventricular heart valve (AHV) leaflets have a complex microstructure composed of four distinct layers: atrialis, ventricularis, fibrosa and spongiosa. Specifically, the spongiosa layer is primarily proteoglycans and glycosaminoglycans (GAGs). Quantification of the GAGs' mechanical contribution to the overall leaflet function has been of recent focus for aortic valve leaflets, but this characterization has not been reported for the AHV leaflets. This study seeks to expand current GAG literature through novel mechanical characterizations of GAGs in AHV leaflets. For this characterization, mitral and tricuspid valve anterior leaflets (MVAL and TVAL, respectively) were: (i) tested by biaxial mechanical loading at varying loading ratios and by stress-relaxation procedures, (ii) enzymatically treated for removal of the GAGs and (iii) biaxially mechanically tested again under the same protocols as in step (i). Removal of the GAG contents from the leaflet was conducted using a 100 min enzyme treatment to achieve approximate 74.87% and 61.24% reductions of all GAGs from the MVAL and TVAL, respectively. Our main findings demonstrated that biaxial mechanical testing yielded a statistically significant difference in tissue extensibility after GAG removal and that stress-relaxation testing revealed a statistically significant smaller stress decay of the enzyme-treated tissue than untreated tissues. These novel findings illustrate the importance of GAGs in AHV leaflet behaviour, which can be employed to better inform heart valve therapeutics and computational models.

1. Introduction

The mitral valve (MV) and the tricuspid valve (TV), also named the atrioventricular heart valves (AHVs), are responsible for regulating unidirectional blood flow from the atria into the ventricles via proper cyclic closing and opening of the valve leaflets. The MV, residing on the left side of the heart, is composed of two leaflets designated by their anatomical locations

Table 1. Nomenclature.

	abbreviation	description
anatomy	AHV	atrioventricular heart valve
	AV	aortic valve
	MV	mitral valve
	MVAL	mitral valve anterior leaflet
	MVPL	mitral valve posterior leaflet
	TV	tricuspid valve
	TVAL	tricuspid valve anterior leaflet
	TVPL	tricuspid valve posterior leaflet
	TVSL	tricuspid valve septal leaflet
leaflet constituent	GAG	glycosaminoglycan
	PG	proteoglycan
	VIC	valvular interstitial cell
mechanics-related	$\mathbf{F}$	deformation gradient tensor
	$\mathbf{C}$	right Cauchy-Green deformation tensor $= \mathbf{F}^T\mathbf{F}$
	$\mathbf{E}$	Green–Lagrange strain tensor $= 0.5\,(\mathbf{C}-\mathbf{I})$
	$\mathbf{I}$	second-order identity tensor
	J	determinant of $\mathbf{F}$ (volume ratio)
	λ_{circ}	stretch in the circumferential direction
	λ_{circ}^{0-peak}	tissue peak stretch in the circumferential direction
	λ_{circ}^{0-1}	preconditioning stretch in the circumferential direction
	λ_{circ}^{1-peak}	mechanical stretch in the circumferential direction
	λ_{rad}	stretch in the radial direction
	λ_{rad}^{0-peak}	tissue peak stretch in the radial direction
	λ_{rad}^{0-1}	preconditioning stretch in the radial direction
	λ_{rad}^{1-peak}	mechanical stretch in the radial direction
	Ω_0	reference configuration (tissue mounting prior to the preconditioning step)
	Ω_1	post-preconditioning configuration
	$\mathbf{P}$	first Piola–Kirchhoff stress tensor
	P_{xx}, P_{yy}	normal components of $\mathbf{P}$ in the x- and y-directions, respectively
	$\mathbf{S}$	second Piola–Kirchhoff stress tensor
	$\boldsymbol{\sigma}$	Cauchy stress tensor
	t	thickness of the tissue specimen
	T_x, T_y	membrane tensions in the x- and y-directions, respectively
specimen label	C	control
	T	treated
tissue's collagen fibre orientation	circ	circumferential direction
	rad	radial direction
other	PBS	phosphate-buffered saline
	DIC	digital image correlation
	s.e.m.	standard error of the mean

as the anterior leaflet (MVAL) and posterior leaflet (MVPL). By contrast, the TV, residing on the right side of the heart, is composed of three tissue leaflets: the anterior leaflet (TVAL), posterior leaflet (TVPL) and septal leaflet (TVSL). The AHV leaflets are complex in their morphological structure, consisting of four distinct layers in an order from the atrial face to the ventricular side as the atrialis, spongiosa, fibrosa and ventricularis [1–3]. The layers are unique in their constituents, with the atrialis and ventricularis consisting of collagen and radially oriented elastin [4–6], the load-bearing fibrosa primarily consisting of circumferentially oriented dense networks of Type I and Type III collagen fibres [3,7], the lubricating spongiosa composed of glycosaminoglycans (GAGs) and proteoglycans (PGs) [8–11], and valvular interstitial cells (VICs) dispersed throughout all four layers (table 1).

Proper leaflet function relies on the valve leaflet tissue's microstructural components, consisting of collagen fibres, elastin fibres, PGs, GAGs and VICs. Maintaining valvular function using surgical reparative techniques is associated with a survival benefit. Moreover, the collagen fibres are found in the atrialis, ventricularis and fibrosa layers and are responsible for the tissue's stiffness and strength, especially in the high-stress states of the valve's systolic closure [12,13]. The elastin fibres are exhibited primarily in the atrialis and ventricularis layers. For the MVAL, it has been shown that the elastin fibres in the ventricularis layer align primarily in the circumferential direction, while those in the atrialis layer align primarily in the radial direction [14,15]. For the aortic valve (AV), the elastin is responsible for the tissue's elasticity at large radial strains when the valve opens and recoiling when the valve closes [5,6,12,13]. The PGs are present in the spongiosa and are responsible for absorbing compressive forces and mediating the collagen and elastin functions [12,13], whereas the GAGs are found throughout the leaflet while being especially dense in the spongiosa and are highly hydrophilic, allowing for reduced shear between the fibrosa and ventricularis layers [16,17]. Additionally, the GAGs have also been found in tendinous tissues to be responsible for time-dependent mechanical behaviours, being the load-bearing constituent in low-stress regimes [18–20]. It has been suggested that this GAG behaviour may be reflected in the heart valve leaflets [21] and that GAGs found in arterial tissues play a significant biomechanical role in both healthy and diseases states [22,23]. VICs are found throughout all four AHV leaflet layers and are responsible for maintaining leaflet structural integrity by protein synthesis and enzymatic degradation, providing unique biomechanical behaviours based on the layer in which they are present [14]. Each of these constituents contributes to the organ-level function of the leaflet, and as such studies have sought to characterize the stress–strain behaviours of heart valve leaflet tissues, and each microstructural constituent's contribution to the tissue's mechanical behaviours.

Previously, the clear zone (belly) portions of both the MV and TV leaflets have been characterized, and the mechanical testing results revealed an anisotropic, nonlinear mechanical response [14,24–30]. In addition to these bulk leaflet investigations, studies have also been focused on more comprehensive analyses of the leaflets' tissue mechanics. For example, the leaflet has been shown to exhibit varying regional deformations and mechanical properties [31–33]. Another study for the AV investigated the mechanical contributions of distinct leaflet tissue layers by a micro-dissection procedure [29]. These studies provided insight into the mechanical characteristics of respective tissue layers: the collagenous fibrosa being the major load-bearing layer, and the atrialis and ventricularis being elastin-rich layers responsible for the tissue's low-stress elasticity. However, the spongiosa layer is composed primarily of GAGs and PGs as well as other non-fibrous matrix substance, making the above micro-dissection technically infeasible for separating the spongiosa for its biomechanical characterizations. Hence, enzymatic constituent removal processes are required to analyse the mechanical contributions of the GAGs and PGs, and these processes have become recent focuses for heart valve biomechanics research.

The PGs and GAGs have been studied *in vitro* through extraction and isolation from cartilage with key observations that the PGs and GAGs exhibit viscous flow-like characteristics, shear-thinning behaviours and non-Newtonian fluid behaviours, demonstrating the constituent as being sensitive to the loading rate [34–36]. Within the scope of heart valve biomechanics, the AV and AHV leaflets have been shown to be loading-rate dependent [24,37–40], which may be behaviours contributed in part by the GAGs. Additionally, the GAGs in heart valve leaflet studies have been shown to play a critical role in collagen fibre recruitments during loading, which in turn gives the tissue its nonlinear stress-stretch behaviour [11,17,21,41]. Other studies have also directly quantified the biomechanical role of the GAGs in AV leaflets through mechanical testing pre- and post-enzymatic treatment [21,42,43]. In these studies, it was found that the GAG removal led to greater AV leaflet tissue flexural rigidity, a greater buckling behaviour and a greater extensibility with respect to the tensile viscoelastic properties as compared to native AV leaflets. It is noted that the AV leaflets have three morphologically distinct layers [6,29], whereas the AHV leaflets have four distinct layers [14,39,44,45]. Such morphological difference suggests that the microstructural interactions may be different between the AV leaflets and AHV leaflets. Nevertheless, quantifications of the GAGs' contributions to leaflet mechanical behaviour have not been made for the AHVs. Thus, there is a need for comprehensive investigations of the GAGs' role in the biaxial mechanical responses and the stress-relaxation behaviour, which will lead to greater refinement of AHV leaflet microstructure knowledge.

The goal of this study is therefore to fill this gap in knowledge through biaxial mechanical characterization of AHV leaflet tissues before and after removal of the GAG constituent. Specifically, the MVAL and TVAL were considered to represent each of the AHVs for their anisotropic, nonlinear nature. Leaflets were tested using biaxial loading and stress-relaxation protocols, enzyme-treated to remove the GAGs, and tested again to observe post-treatment differences in the mechanical response. Findings of this study will contribute to the existing literature regarding microstructural characterizations of heart valve leaflets.

2. Material and methods

2.1. Tissue acquisition and preparation

Healthy porcine hearts (80–140 kg of weight, 1–1.5 years of age, 1 : 1 female-to-male ratio) were obtained from a local USDA-approved abattoir (Country Home Meat Company, Edmond, OK) on the same day as animal slaughter. Upon arrival to the laboratory, blood clots were cleaned from the valves. This cleaning procedure involved rinsing the heart in phosphate-buffered saline (PBS) solution, making incisions along the parting line between the atria and ventricles to reveal the AHVs, and then using forceps to remove blood clots from the ventricles. Once hearts were fully cleaned of blood clots, they were frozen at -14°C for prolonged storage time before subsequent biaxial mechanical testing. Freezing of heart samples was used based on previous studies, which was shown in practice to induce negligible effects of freezing on the quantified mechanical properties of skin and arterial tissues [46,47].

Frozen hearts were thawed at the time of dissection of both the MVAL and TVAL. The central portions of the excised leaflets were sectioned into 10×10 mm specimens (figure 1*a*). Three thickness measurements of the sectioned leaflet were taken via

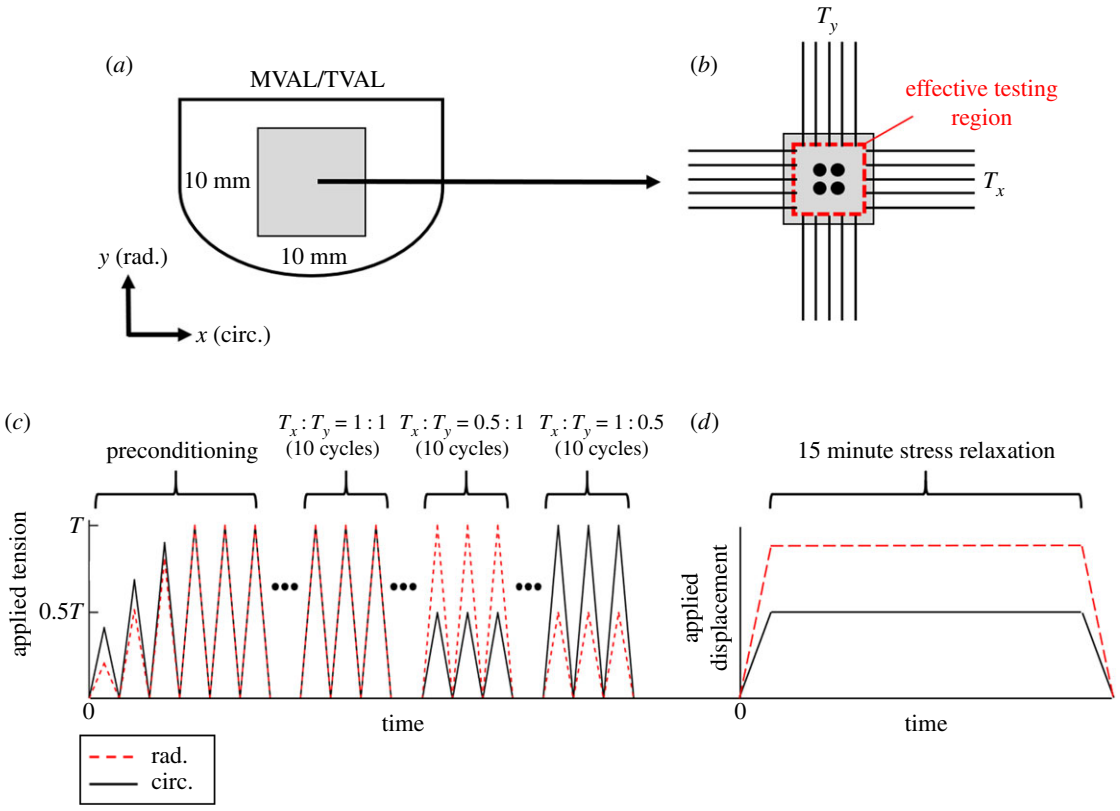

Figure 1. (*a*) Dissection of the mitral valve and tricuspid valve anterior leaflets into 10 × 10 mm specimens; (*b*) experimental set-up for biaxial mechanical testing of the MVAL and TVAL tissue specimens. Schematic of the testing procedures: (*c*) force-controlled biaxial testing protocol; (*d*) biaxial stress-relaxation testing protocol. (Online version in colour.)

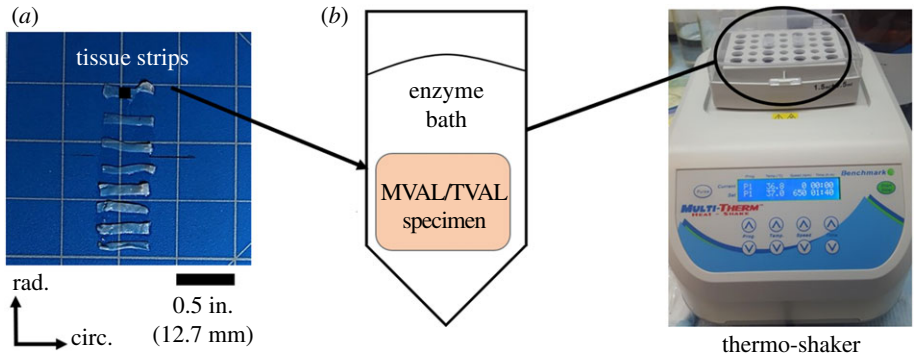

Figure 2. Schematic of the enzyme-based GAG removal treatment: (*a*) tissue strips of the MVAL or the TVAL used for the determination of optimal treatment; (*b*) tissue specimen (either the tissue strip, used for histology, or the square tissue, used for biaxial mechanical testing) in a 1.5 ml vial with enzyme bath at 37°C. (Online version in colour.)

a digital caliper (Westward 1AAU4—0.01 mm resolution) and the measurements averaged to account for regional variations in tissue thickness. The specimens then underwent biaxial mechanical testing and the enzyme treatment within 48 h of heart harvesting (cf. §§2.2 and 2.4).

2.2. GAG degradation treatment

To examine the GAG contributions to AHV leaflet tissue mechanics, force-controlled and stress-relaxation biaxial mechanical tests were performed prior to and after an enzyme-based GAG degradation procedure previously developed for the AV leaflets [21]. In brief, an enzyme solution consisting of 30 U ml^{-1} of the enzyme hyaluronidase type VI-S and 0.6 U ml^{-1} of the enzyme chrondroitinase ABC from *Proteus vulgaris* (Sigma Aldrich no. H3631 and no. C3667) in 100 mM ammonium acetate buffer solution (AABS, Sigma Aldrich no. A1542) was prepared with an adjusted pH of 7.0. The MVAL or TVAL tissue specimen was placed in a 1.5 ml microvial tube filled with the prepared GAG degradation solution and continuously shaken (H5000-H MultiTherm Shaker, Benchmark Scientific, Sayreville, NJ) for the optimal enzyme treatment time (as described below) at 37°C (figure 2). The enzyme solution was then removed and the leaflet tissue specimen was washed with ice-cold PBS three times, for 5 min each time.

Since such an enzyme treatment procedure has not been used for investigations of the GAG degradation of both the MV and TV leaflets (which have a distinct difference in tissue thicknesses from the AV), an intermediate study was conducted to determine the optimal enzyme treatment time. The optimal time was considered as a balance between the amount of GAGs degraded (greater than 50%) and the experimental time. Briefly, porcine MVAL and TVAL leaflets were sectioned into tissue strips (figure 2*a*), with one strip from each untreated leaflet serving

as the control and all other tissue strips subjected to the above-mentioned enzyme-based GAG degradation procedure. Tissue strips were continuously shaken in the enzyme degradation solution with one tissue strip from each leaflet removed every 20 min until a final time point of 160 min (figure 2*b*). After all tissue strips had been treated and PBS-washed, histological analysis was then performed (cf. §2.3) to quantify the percentage of GAGs remaining at each time point. The percentage GAG reduction was then computed at each time point with respect to the control slide to determine the treatment time associated with at least 50% GAG removal. This optimal treatment time of 100 min, determined by the GAG content quantification as described in §2.3, was used in subsequent biaxial testing procedures (cf. §2.4).

2.3. Histological preparation and GAG content quantification

Routine histological preparations of the paraffin-embedded tissue strips were performed (fixed 24 h in 10% neutral buffer formalin, one tissue strip for each time point) to quantify the progression of GAG degradation under continued enzyme treatment. To visualize and identify GAG contents, Alcian blue staining was used [42,43]. In brief, 5 µm thick paraffin sections were deparaffinized and hydrated with distilled water, mordant in 3% aqueous acid for 3 min, thoroughly rinsed, then dehydrated for subsequent mounting and coverslipping and finally stained by Alcian blue stains.

Four digital micrographs were taken for each of the stained tissue strips using an inverted bright-field microscope (Olympus, Tokyo, Japan) with a 10× or 4× objective lens for the TVAL and MVAL, respectively, and a 10 mega-pixel camera. Images were then analysed using ImageJ (NIH, Bethesda, MA) and the Colour Deconvolution plug-in [48] to determine the percentage of GAGs in each image. This per cent GAG content value was then averaged for the four images at each time point to account for the regional variations within the tissue strip. The per cent GAG content at each time point was then compared to the untreated (control) sample, taken from the same valve leaflet tissue, to determine the per cent GAG reduction. The optimal treatment time was determined when the majority of the leaflet's GAG content (greater than 50%) had been removed, and further treatment did not result in a significant degradation of the GAG content. Additionally, the tissue thickness was determined for each image and averaged at each time point.

2.4. Biaxial mechanical testing

For biaxial mechanical testing, the previously prepared MVAL or TVAL specimen (cf. §2.1) was mounted using a set of 4 BioRake tines to a commercial biaxial testing system (BioTester–CellScale, Canada) equipped with a 1.5 N capacity load cell and a high-resolution CCD camera. The tissue's circumferential direction, with which the majority of collagen fibres are oriented, was aligned with the testing x-direction while the radial direction was aligned with the testing y-direction (figure 1*a*,*b*). After mounting, four fiducial markers were placed using a surgical pen in a square array on the central region of the leaflet for later digital image correlation (DIC) methods (cf. §2.5). The specimen was then submerged in PBS solution at 37°C to mimic the AHV's physiological condition.

For quantification of the GAG contribution to the overall leaflet's mechanical behaviour, a sequential biaxial mechanical testing procedure was performed, including: (i) control testing—biaxial mechanical testing of the untreated (control, denoted by -C) MVAL or TVAL specimen with an effective testing region of size 7×7 mm; (ii) GAG degradation—enzymatic removal of GAGs (figure 2) using the optimal treatment time, as determined in §2.2, with the tissue specimen unmounted from the biaxial testing system; (iii) post-GAG removal testing—biaxial mechanical testing of the enzyme-treated specimen (denoted by -T) with an effective testing region of size 5.5×5.5 mm to avoid interference with BioRake insertion points from previous mounting. The biaxial mechanical testing performed before and after GAG removal (figure 1*c*,*d*) consists of (i) a force-controlled biaxial mechanical testing protocol previously developed by our group [39] with a preconditioning step, followed by 10 loading/unloading cycles at various circumferential-to-radial membrane tension ratios ($T_x : T_y = 1:1$, $0.5:1$ and $1:0.5$) at a loading rate of 4.42 N min^{-1}, and (ii) a 15 min biaxial stress-relaxation testing protocol with constant displacements corresponding to the tissue's specific deformation associated with targeted membrane tension. Ten loading–unloading cycles were used for each loading ratio to ensure repeatability of the stress–stretch curves, and data analysis was performed using the final cycle. This modified three-step mechanical characterization procedure allowed for investigations of GAG constituent's contribution to the MVAL and TVAL biomechanics using one single tissue specimen before and after GAG removal.

Note that tissues were loaded, based on their *effective edge length*, to a targeted membrane tension of 100 and 75 N m^{-1} for the MVAL and TVAL, respectively, according to its physiological pressure loading condition [27,49]. In all the biaxial mechanical tests, the BioRake separation distance, load cell force readings, and images of the marker positions were continuously captured at a rate of 15 Hz for use in the tissue stress and strain calculations outlined in the next section.

2.5. Biaxial data analyses—tissue stress and strain calculations

For a more detailed description of the tissue strain and stress calculations employed, refer to our previous publications [26,39]. Briefly, we used the DIC functionality of the LabJoy software of the BioTester system to obtain time-dependent positions of the four fiducial markers. The time-dependent marker positions were then used to compute the deformation gradient $\mathbf{F}$, and subsequently, the principal stretches in the circumferential and radial directions (λ_{circ} and λ_{rad}). The membrane tensions (T_x and T_y) associated with each deformation gradient were computed using the load cell's force reading and each specimen's effective testing region edge length. From the membrane tensions, other measures of stress may be calculated using the specimen's thickness: $\mathbf{P} = \text{diag}[P_{XX}, P_{YY}] = \text{diag}[T_x, T_y]/t$, $\mathbf{S} = \mathbf{F}^{-1}\mathbf{P}$, and $\boldsymbol{\sigma} = J^{-1}\mathbf{P}\mathbf{F}^{T}$ [50,51]. Herein $\mathbf{P}$ is the first Piola–Kirchhoff stress tensor, $\mathbf{S}$ is the second Piola–Kirchhoff stress tensor, σ is the Cauchy stress tensor and J is the Jacobian of $\mathbf{F}$. For the biaxial stress-relaxation testing, force values were converted to membrane tensions and normalized with respect to the maximum membrane tension in each direction to examine the stress-reduction behaviour of both the MVAL and TVAL tissues between the control and treated groups.

2.6. Statistical analysis

Results are represented as the mean ± s.e.m. (the standard error of the mean). Each dataset was plotted on a quantile–quantile (Q–Q) plot to observe the normality of the experimental data (electronic supplementary material, figure S1–S4). In general, these plots demonstrated a linear relationship, but there were several cases with outliers from this linear relationship. Thus, the non-parametric Mann–Whitney U test was performed to determine the statistically significant differences between the control and enzyme-treated groups of both the MVAL ($n = 7$)

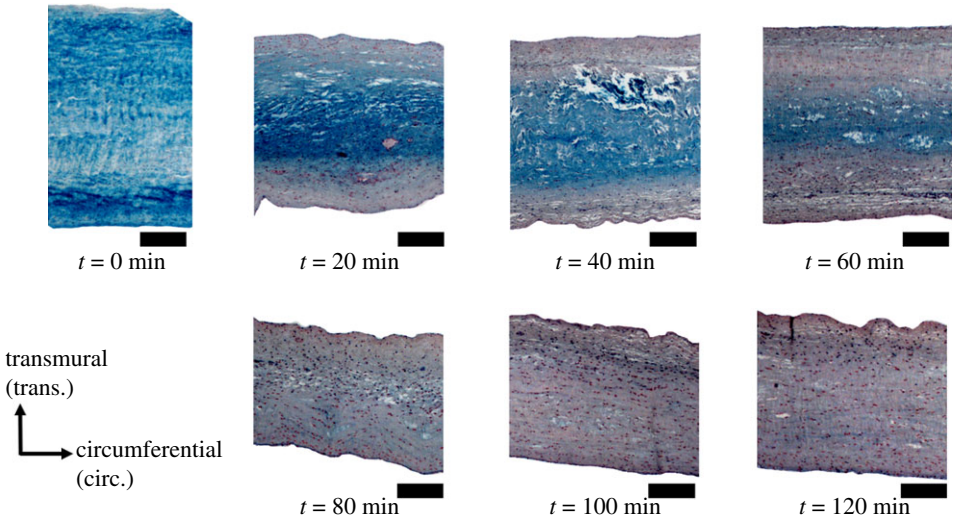

Figure 3. Alcian blue-stained histological images demonstrating the progression of the GAG constituent removal associated with various enzyme treatment durations. Scale bar = 200 µm. (Online version in colour.)

Table 2. Percentage of glycosamnioglycans in the control and enzyme-treated tissue strips over a 160 min treatment time. Results of time = 0 min refer to the untreated (control) tissue. All quantities are reported as mean ± s.e.m.

	MVAL		TVAL	
time (min)	GAGs in tissue strip (%)	GAG reduction w.r.t. control (%)	GAGs in tissue strip (%)	GAG reduction w.r.t. control (%)
0 (control)	82.23 ± 3.85	—	45.16 ± 1.08	—
20	47.43 ± 2.31	42.32	16.94 ± 2.57	62.49
40	36.83 ± 3.33	55.32	11.66 ± 0.64	74.19
60	27.20 ± 2.52	66.92	14.31 ± 0.88	68.30
80	31.63 ± 1.52	61.53	13.11 ± 1.10	70.97
100	19.81 ± 1.62	75.91	17.50 ± 0.93	61.24
120	17.70 ± 1.46	78.48	11.63 ± 1.04	74.24
140	21.36 ± 1.40	74.02	17.61 ± 1.23	61.00
160	24.99 ± 1.76	69.60	17.32 ± 1.99	61.65

and TVAL ($n = 6$) tissue specimens. Following the analysis procedure in our previous work [26,39], the statistical analyses were performed considering: (i) the *peak tissue stretches* (λ_{circ}^{0-peak} and λ_{rad}^{0-peak}) associated with the peak membrane tensions with respect to the reference configuration Ω_0 where the tissue was mounted; (ii) the *preconditioning stretches* (λ_{circ}^{0-1} and λ_{rad}^{0-1}), defined as the tissue deformations between Ω_0 and the post-preconditioning configuration Ω_1, primarily due to the preconditioning effect; (iii) the *mechanical stretches* (λ_{circ}^{1-peak} and λ_{rad}^{1-peak}), defined as the tissue deformation due to mechanical loading with respect to Ω_1. Moreover, the anisotropy index (AI), defined as the ratio between λ_{circ}^{0-peak} and λ_{rad}^{0-peak}, was calculated. The null hypothesis for our statistical analyses was that the mean of the difference between these two groups had a value of zero, i.e. GAG removal had no statistically significant effect on the tissue mechanics.

In addition, comparison of the stress-relaxation data followed a similar statistical analysis method. Normalized membrane tensions at the end of the 15 min interval were compared to determine if there was a significant difference in the stress-relaxation behaviour before and after the enzymatic treatment. For all the statistical analyses, $p < 0.05$ was considered to be *statistically significant*.

3. Results

3.1. Histological evaluations of glycosaminoglycan progressive degradation

Results from the histological analyses for both the MVAL and TVAL are provided in table 2 with histological images of the progressive GAG degradation provided in figure 3. For the MVAL tissue, the enzyme treatment resulted in a gradual reduction of the GAG constituent increasing with time until the 60 min time point (66.92% removed). Variations in the GAG reduction trend observed after the 80 min time point are expected to result from regional heterogeneities in the microstructural quantities. Regardless, the treatment reached the desired threshold of greater than 50% GAG constituent removed at the 40 min time point (53.27% removed). The TVAL showed a more rapid reduction of GAGs, reaching 74.19% reduction in GAGs within 40 min. After the 40 min time point, the percentage of GAG removal fluctuated between 61% and 74%. This may be attributed to the expected regional heterogeneities in the tissue's

Table 3. Control (C-) and enzyme-treated (T-) leaflet testing parameters, including the applied membrane tension, the effective edge length, the applied force, the thickness (obtained using the caliper-based approach detailed in §3.2) and the total specimen edge length.

valve leaflet	condition	membrane tension (N m^{-1})	effective edge length (mm)	applied force (mN)	thickness (mm)	total edge length (mm)
MVAL323	C-	100	7.0	700	0.55	10.0
	T-	100	5.5	550	0.19	8.5
MVAL324	C-	100	7.0	700	0.43	10.0
	T-	100	5.5	550	0.34	8.5
MVAL325	C-	100	7.0	700	0.63	10.0
	T-	100	5.5	550	0.42	8.5
MVAL327	C-	100	7.0	700	0.42	10.0
	T-	100	5.5	550	0.34	8.5
MVAL328	C-	100	7.0	700	0.56	10.0
	T-	100	5.5	550	0.51	8.5
MVAL329	C-	100	7.0	700	0.48	10.0
	T-	100	5.5	550	0.41	8.5
MVAL330	C-	100	7.0	700	0.45	10.0
	T-	100	5.5	550	0.32	8.5
TVAL323	C-	75	7.0	525	0.31	10.0
	T-	75	5.5	412.5	0.16	8.5
TVAL324	C-	75	7.0	525	0.16	10.0
	T-	75	5.5	412.5	0.15	8.5
TVAL325	C-	75	7.0	525	0.53	10.0
	T-	75	5.5	412.5	0.30	8.5
TVAL326	C-	75	7.0	525	0.19	10.0
	T-	75	5.5	412.5	0.14	8.5
TVAL327	C-	75	7.0	525	0.25	10.0
	T-	75	5.5	412.5	0.15	8.5
TVAL328	C-	75	7.0	525	0.25	10.0
	T-	75	5.5	412.5	0.17	8.5
TVAL329	C-	75	7.0	525	0.19	10.0
	T-	75	5.5	412.5	0.17	8.5
TVAL330	C-	75	7.0	525	0.17	10.0
	T-	75	5.5	412.5	0.15	8.5

microstructure [33]. To account for variations between specimens and to ensure that the treatment met the desired threshold (greater than 50% GAGs removed), the optimal treatment time for both the MVAL and TVAL was selected to be 100 min.

3.2. Thickness measurements

Thicknesses of the tissue leaflets, to be used for biaxial testing, before and after enzyme treatment were recorded using the digital caliper method, revealing a 20–30% reduction in tissue thickness after treatment: MVAL-C, 0.50 ± 0.03 mm; MVAL-T, 0.36 ± 0.04 mm; TVAL-C, 0.25 ± 0.04 mm; TVAL-T, 0.18 ± 0.02 mm. Tissue thickness measurements for all specimens are provided in table 3.

3.3. Results of force-controlled biaxial mechanical testing

Comparing the control and enzyme-treated groups with regard to the equibiaxial loading ratio ($T_x : T_y = 1:1$), it was observed that the GAG-degraded specimens experienced greater stretches than the control specimens in both the circumferential and radial directions. First, comparing the peak tissue stretches between the control and treated groups, both the circumferential and radial directions experienced greater stretch values post treatment. The per cent difference in $\lambda_{\mathrm{circ}}^{0-\mathrm{peak}}$ was 5.4% for the MVAL ($p = 0.038$) and 4.7% for the TVAL ($p = 0.132$), whereas the per cent difference in $\lambda_{\mathrm{rad}}^{0-\mathrm{peak}}$ was 5.3% for the MVAL ($p = 0.165$) and 7.6% for the TVAL ($p = 0.015$) (figure 4*a* and figure 5*a*). Similar trends in the peak stretch were observed for the non-equibiaxial loading protocols (figure 4*b*,*c* and

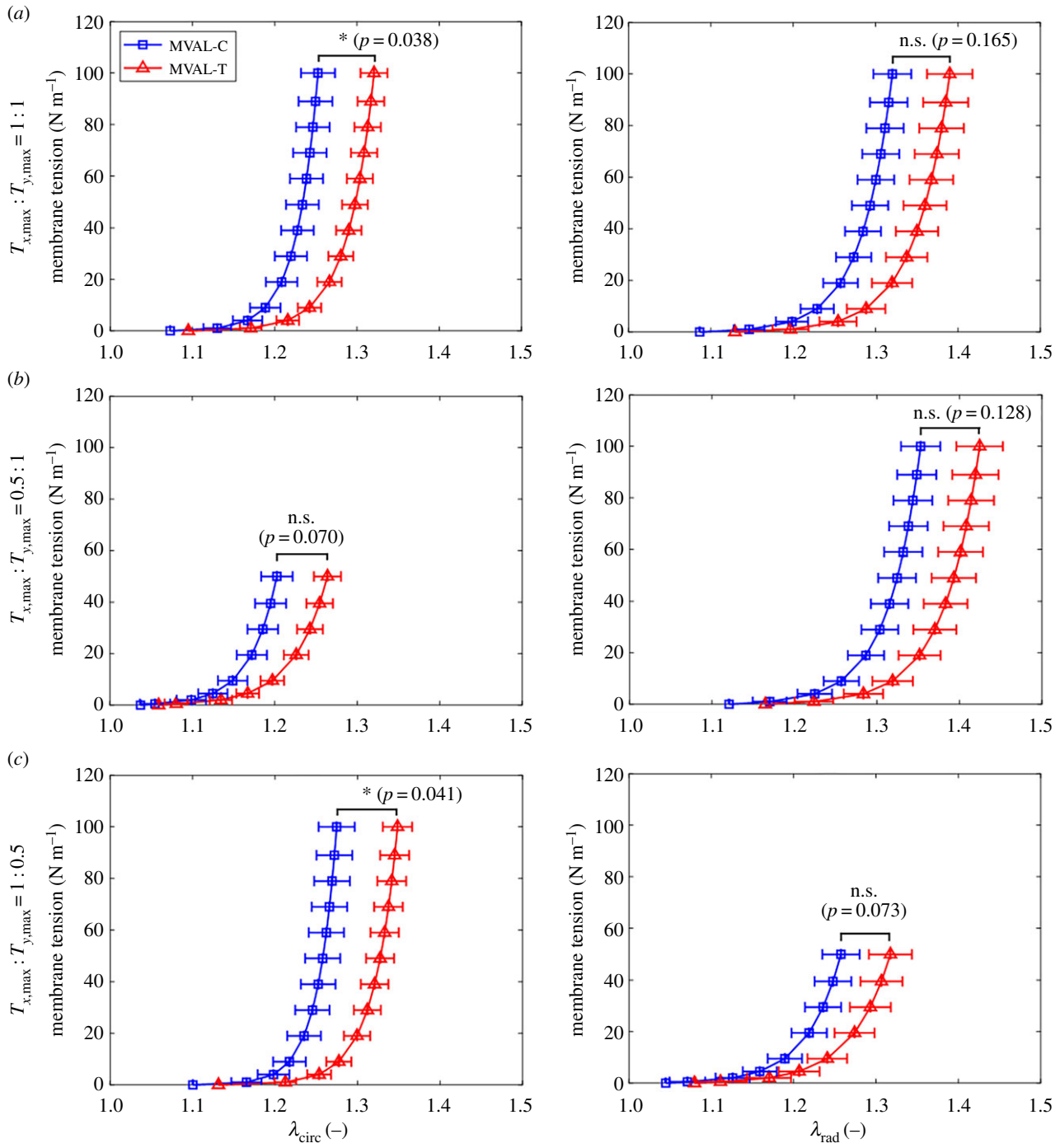

Figure 4. Mean ± s.e.m. of the peak tissue stretch responses of the control and enzyme-treated groups for the MVAL ($n = 7$): $T_x : T_y = (a)$ 1 : 1, (b) 0.5 : 1 and (c) 1 : 0.5. (*: statistically significant; n.s.: statistically non-significant). (Online version in colour.)

figure 5*b*,*c*). In the $T_x : T_y = 0.5 : 1$ loading protocol, a significant difference in both λ_{circ}^{0-peak} ($p = 0.041$) and λ_{rad}^{0-peak} ($p = 0.026$) was observed for the TVAL. As for the $T_x : T_y = 1 : 0.5$ loading protocol a significant difference was found in λ_{circ}^{0-peak} for the MVAL ($p = 0.041$) and in λ_{rad}^{0-peak} for the TVAL ($p = 0.002$). Additionally, the peak stretch values for the equibiaxial protocol were further used to compare the anisotropy index. The MVAL tissues demonstrated minimal change between the control and treated AI values (1.055 ± 0.022 versus 1.052 ± 0.022; $p = 0.902$), while a slight increase in AI (1.031 ± 0.017 versus 1.059 ± 0.028; $p = 0.556$) was observed for the TVAL tissues.

Secondly, the preconditioning stretches were shown to be greater post-treatment for both the circumferential and radial directions. Specifically, the per cent difference in λ_{circ}^{0-1} was 2.1% greater for the MVAL ($p = 0.274$) and 2.7% greater for the TVAL ($p = 0.310$) (figure 6*a* and figure 7*a*). The per cent difference in λ_{circ}^{0-1} was 3.9% greater for the MVAL ($p = 0.365$) and 4.8% greater for the TVAL ($p = 0.048$, *statistically significant*) (figure 6*b* and figure 7*b*). Finally, the mechanical stretches were greater at post-treatment for both the MVAL and TVAL. The per cent difference in λ_{circ}^{0-peak} was 3.3% for the MVAL ($p = 0.058$) and 2.0% for the TVAL ($p = 0.240$), respectively, while the per cent difference in λ_{rad}^{1-peak} was 1.2% for the MVAL ($p = 0.515$) and 2.6% for the TVAL ($p = 0.329$) (figure 8*a* and figure 9*a*). Similar trends of increasing the mechanical stretch post-treatment were observed for the non-equibiaxial loading protocols (figure 8*b*,*c* and figure 9*b*,*c*).

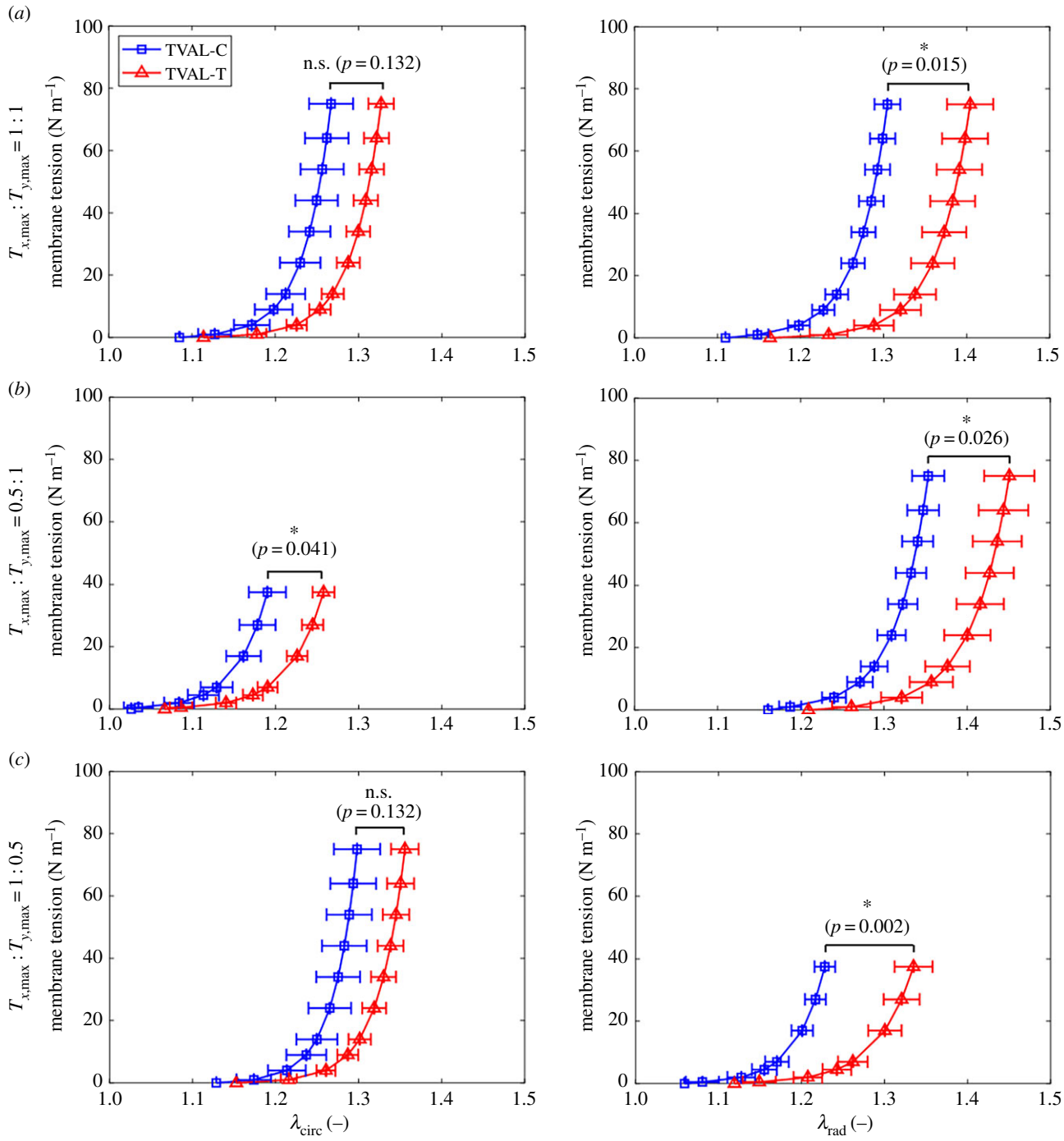

Figure 5. Mean ± s.e.m. of the peak tissue stretch responses of the control and enzyme-treated groups for the TVAL ($n = 6$): $T_x : T_y =$ (*a*) 1 : 1, (*b*) 0.5 : 1 and (*c*) 1 : 0.5. (*: statistically significant; n.s.: statistically non-significant). (Online version in colour.)

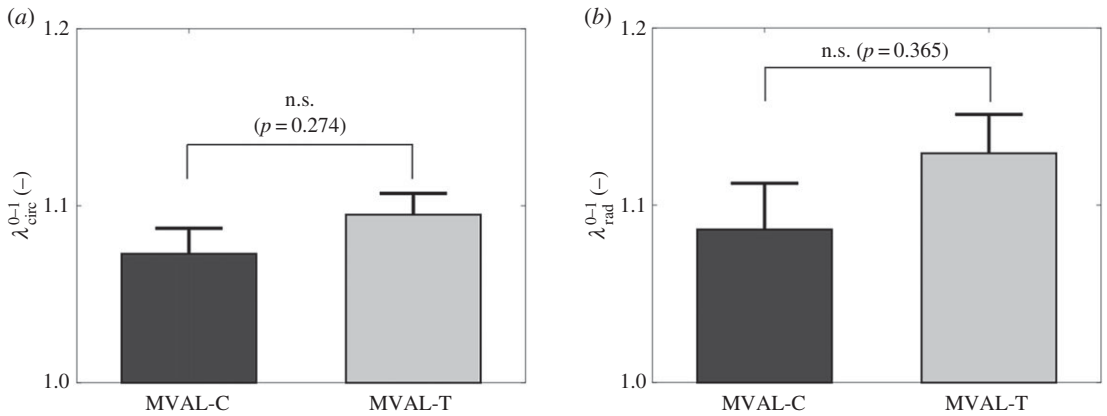

Figure 6. Comparison of the preconditioning stretches (mean ± s.e.m.) of the MVAL between the control and enzyme-treated groups in the (*a*) circumferential, and (*b*) radial directions. (n.s.: statistically non-significant).

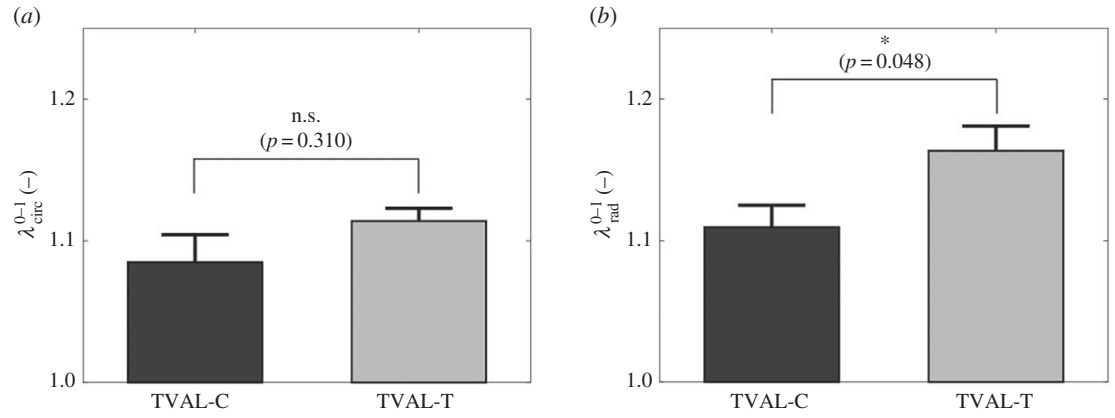

Figure 7. Comparison of the preconditioning stretches (mean ± s.e.m.) of the TVAL between the control and enzyme-treated groups in the (*a*) circumferential, and (*b*) radial directions. (*: statistically significant; n.s.: statistically non-significant).

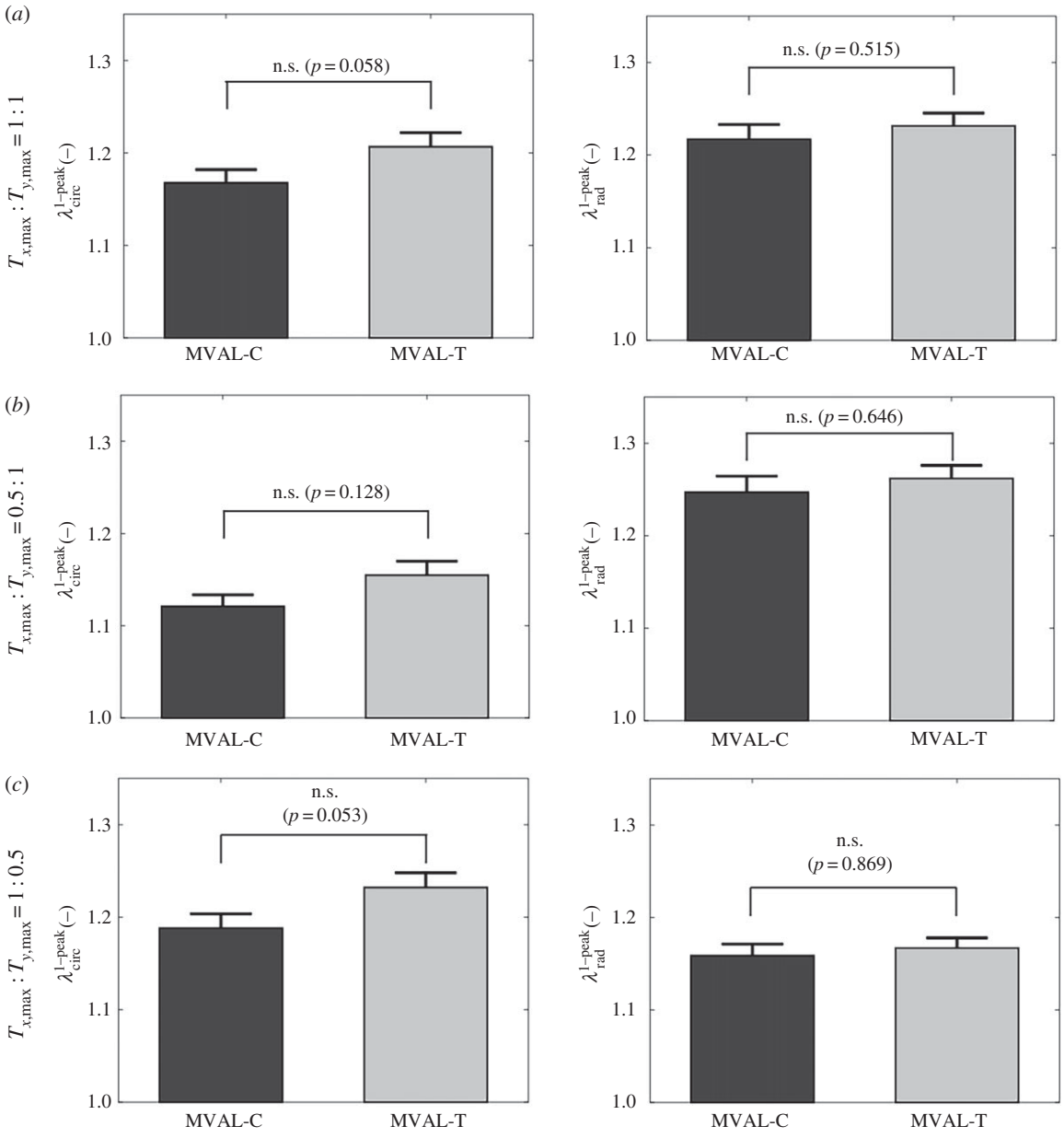

Figure 8. Comparison of the mechanical stretches (mean ± s.e.m.) of the MVAL between the control and enzyme-treated groups: $T_x : T_y =$ (*a*) 1 : 1, (*b*) 0.5 : 1; (*c*) 1 : 0.5. (n.s.: statistically non-significant).

3.4. Results of stress-relaxation testing

The average, normalized membrane tension reductions for the treated and untreated (control) specimens are presented in figure 10*a,b* for the MVAL and figure 11*a,b* for the TVAL. It was found that the control tissues had a larger stress reduction than the treated tissues in both directions for the MVAL. In the circumferential direction, there was an observed statistically significant difference

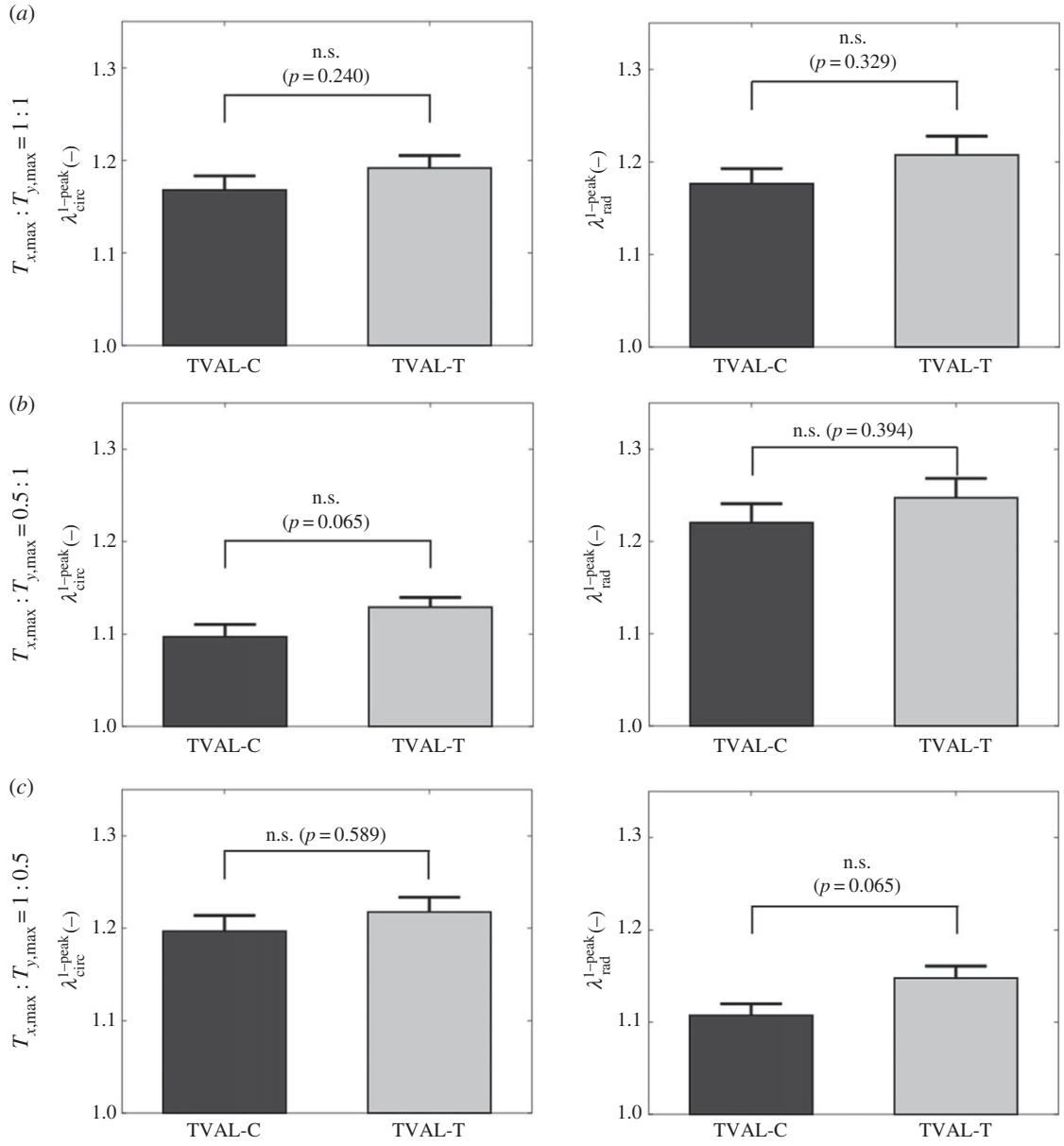

Figure 9. Comparison of the mechanical stretches (mean ± s.e.m.) of the TVAL between the control and enzyme-treated groups: $T_x : T_y$ = (*a*) 1 : 1, (*b*) 0.5 : 1; (*c*) 1 : 0.5. (n.s.: statistically non-significant).

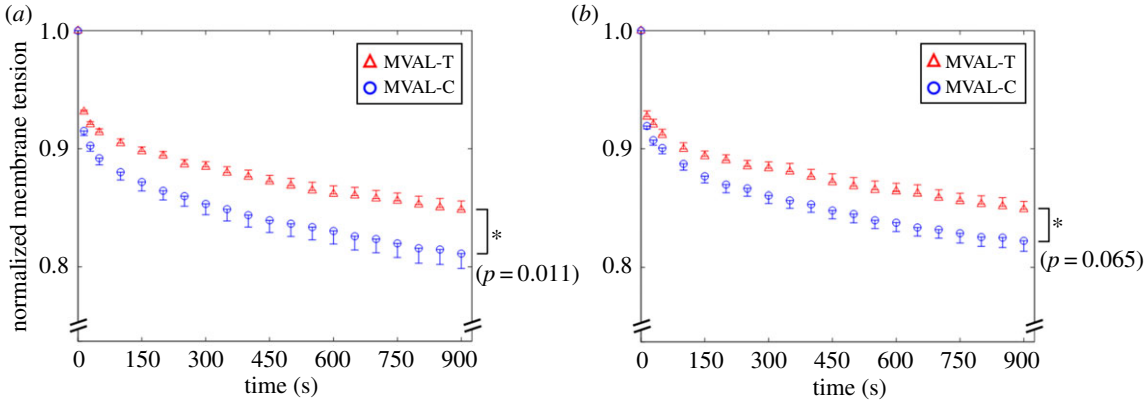

Figure 10. Comparison of the 15 min biaxial stress-relaxation responses (mean ± s.e.m.) of the MVAL between the control and enzyme-treated groups: (*a*) circumferential; (*b*) radial directions. (*: statistically significant). (Online version in colour.)

in the pre- and post-treatment stress relaxation (C: 18.9% relaxation, T: 15.2% relaxation, $p = 0.011$). In the radial direction, there was an observed statistically significant difference in the pre- and post-treatment stress-relaxation behaviours (C: 17.8% relaxation, T: 15.1% relaxation, $p = 0.026$). As for the TVAL tissue specimens, the difference in the stress relaxation was less pronounced. Specifically, there was an approximately 13% difference in the pre- and post-treatment stress-relaxation behaviours in the circumferential direction (C: 17.1% relaxation, T: 15.0% relaxation, $p = 0.065$) and

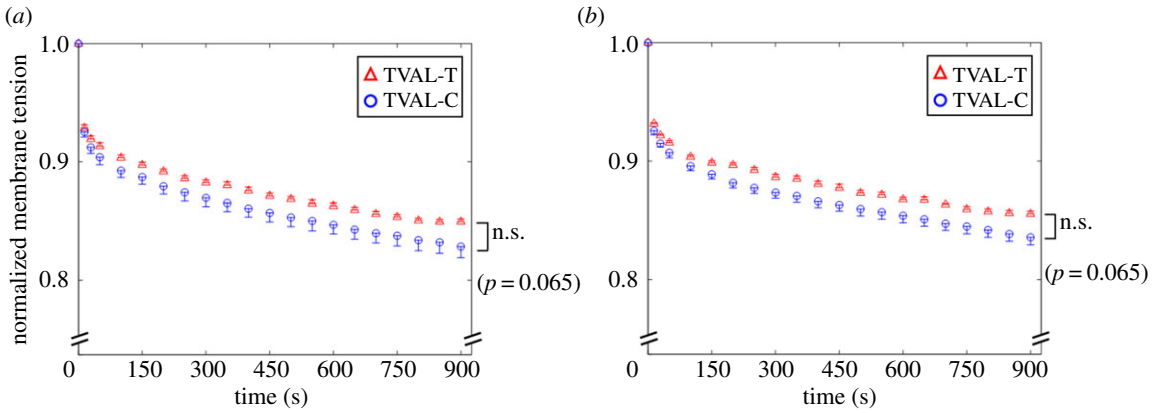

Figure 11. Comparison of the 15 min biaxial stress-relaxation responses (mean ± s.e.m.) of the TVAL between the control and enzyme-treated groups: (*a*) circumferential; (*b*) radial directions. (n.s.: statistically non-significant). (Online version in colour.)

an approximately 12% difference in the radial direction (C: 16.4% relaxation, T: 14.5% relaxation, $p = 0.065$).

4. Discussion

4.1. Overall findings

Biaxial mechanical testing revealed that removal of the GAGs resulted in a statistically significant increase in the peak tissue stretch in both the circumferential and radial directions of the MVAL and TVAL. Decomposing the peak tissue stretch into the preconditioning and mechanical stretches, significant differences were observed for the preconditioning stretch in the radial direction of the TVAL, and for the mechanical stretch in the circumferential direction of the MVAL. One possibility for the greater stretch in the tissue post-treatment may be due to lessened fibre recruitments that are caused by a deficiency of GAGs in the tissue [11,17,21]. Stress-relaxation testing also provided insight into the GAG mechanical contributions, where treated specimens showed a smaller stress decay than untreated specimens (figures 10 and 11). This difference was greater in the MVAL than the TVAL, suggesting that those constituents have a greater stress decay potential in the MV than the TV. These degressions in the stress-relaxation behaviour post-enzymatic treatment suggest that the GAGs contribute to the viscoelastic properties of the AHV leaflets.

Previous studies of GAG contribution to heart valve leaflet function have been performed primarily on the AV leaflets. In these studies, it was found that GAG removal from the AV leaflets resulted in a greater buckling behaviour, a greater flexural rigidity and differences in tensile viscoelastic properties [21,42,43]. In another prior study [10], AV leaflets subject to enzymatic GAG removal were shown to have a greater extensibility, but the results were not statistically significant. In our study, it was found that a removal of GAGs from the MVAL and TVAL resulted in statistically significant changes in extensibility and stress decay. The greater contribution of GAGs could be attributed to the difference in the AV and AHV leaflet structures, as the AV leaflets do not contain the atrialis layer present in the AHV leaflets. One potential rationale regarding the increase in the radial preconditioning stretch and the circumferential mechanical stretch could stem from tissue layer interactions, which are compromised with the lack of spongiosa contribution [21]. To elaborate, one could think of the spongiosa's lubricating function between the fibrosa and atrialis as providing the coupling between the fibres of these layers during the mechanical function. With the removal of one primary component of the spongiosa, the coupling functions could be compromised in some manner that affects how loading is dispersed between the fibrosa and atrialis.

This study has successfully provided insight into the previously uninvestigated mechanical contribution of the GAGs to AHV leaflet function. The findings of this study suggest that GAGs play a critical role in the tensile viscoelastic properties of AHV leaflets. Specifically, it may suggest that GAGs are responsible for regulating the extensibility of the tissue, acting as a mediator between the atrialis and fibrosa layers. These findings also suggest that GAGs are important to the proper function of the AHV leaflets, and a GAG deficiency in those leaflets can significantly increase tissue extensibility, which could lead to inadvertent effects such as valvular heart disease. This information could guide the development of heart valve therapeutics.

One example is the construction of bioprosthetic heart valves, where GAG loss in porcine tissue graft transport is a primary concern [10,17]. Another example is tissue-engineered heart valves where it has been hypothesized that a mismatch of the constituents leads to long-term degradation [52–55]. This mismatch is also seen in human valves with increasing ages, which might be likely corresponding to natural valve degeneration [56]. This information could also be used in computational modelling, where multi-scale models considering the linkage from microstructure functions to macro-scale organ-level functions can lead to more accurate simulations of full valve operation. Specifically, these models may also be refined for predictive, highly accurate patient-specific heart valve simulations that may guide surgical repair methods for each patient's unique pathologies.

4.2. Study limitations and future extensions

There are several limitations to this study. First, the GAGs were not completely removed during the enzymatic treatment procedure; however, the majority (greater than 50%) of GAGs were removed by our experimental procedure for the MVAL and TVAL tissues, and statistically significant differences in the tissues' mechanical responses were observed in both biaxial mechanical testing and the biaxial stress relaxation. Additionally, our recent study [33] demonstrated regional variances in the AHV mechanical responses and leaflet thickness, which suggests heterogeneous

variations in the tissue's microstructure that may have different influences on the enzymatic treatment of each leaflet. Nevertheless, in this study, a treatment time was chosen to ensure greater than 50% of the GAGs were removed (cf. §2.2 and §3.1). Secondly, the enzyme-treated samples had a smaller effective specimen size in comparison to the control (5.5 versus 7 mm). Unpublished preliminary investigations by our laboratory suggest that the change in the specimen size (from 7 to 5.5 mm) induces minimal variations on the observed mechanical properties, as compared to the changes caused by the GAG removal. Third, it was assumed that the central one-third of the tissue delimited by the four fiducial markers (cf. §2.4 and figure 1*b*) experienced homogeneous deformations. The calculations of the tissue's deformation within this region were also assumed to have negligible shear stress that may arise from improper alignment of the BioRake attachments. Fourth, caliper-based thickness measurements presented in this study depend on the amount of force applied during the measurement. In our previous study, we have shown that the dial caliper method agreed considerably with the thickness measurements obtained using histological methods (cf. table 6 and fig. 10 Ref. [39]). Fifth, we used a 15-min hold time for the stress-relaxation testing. Previous studies have shown that 4-h may be more appropriate to explore the full relaxation behaviour [12,38,57]. By contrast, for our study, the 15-min time frame was able to successfully capture the statistically significant difference in the membrane tension reduction between the two study groups. Finally, the mechanical characterizations in this study used porcine hearts, which may not be the most accurate representation of elderly human diseased hearts.

Results of this study have shown that GAGs play a significant role in the tensile viscoelastic properties of AHV leaflets, thus necessitating future investigations. Possible future investigations may be warranted to determine more effective enzymes to be used for GAG removal, or a study involving a treatment of the tissues until full GAG removal. Other possible future investigations include quantification of GAG contribution to the coupling effect between the atrialis and fibrosa layers, and to the AHV leaflet behaviour in those other leaflets not tested in this study. The GAG contributions to the AHV leaflet shearing properties could also be investigated using a testing scheme that subjects the tissue to pure shear conditions. Future studies could also be warranted to investigate the effect of GAG removal on collagen fibre recruitment using the dynamic collagen microstructure imaging technique [58]. A study of this nature could also be useful in analysing the low-stress microstructural behaviours of the tissue pre- and post-GAG removal.

4.3. Conclusion

By studying the effects of the GAGs on overall leaflet mechanical function, a novel contribution has been made to detailing the complex microstructure of the AHV leaflets. It was found that the GAGs play a notable role in the mechanical characteristics of the MVAL and TVAL. Specifically, our results demonstrated: (i) under biaxial mechanical testing, tissues with GAGs removed had greater extensibility; (ii) under stress-relaxation tests, tissues with GAGs removed had a lessened stress decay behaviour. Because of the differences observed in untreated and enzyme-treated specimens, future investigations may be warranted into the GAG contributions of the other AHV leaflets' mechanical behaviours. Findings from this study will be useful in expanding the understanding of the leaflet microstructure that may be used in the refinement of computational models of the AHV. Specifically, this information can be used, with moderate future extensions, for refining existing microstructure-based constitutive models [14,45,59–68] or a growth and remodelling framework for soft tissues [69,70]. These models could then be employed for predictive simulations of the AHV function and to inform improved valve replacement therapeutics.

Data Accessibility. The experimental data from the biaxial mechanical tests of the tissue of all the mitral valve anterior leaflet (MVAL) and tricuspid valve anterior leaflet (TVAL) given in table 3 and figures 4 and 5 can be downloaded from doi:10.6084/m9.figshare.8179556 [71]. Computational analysis-derived results presented in figures 6–8 are reproducible from the provided experimental data.

Authors' Contributions. C.-H.L., A.R.B., R.A.T., A.M., H.M.B. conceived of the study, designed the study, coordinated the study; C.J.R., J.R., L.E.E., E.G.B. carried out the biaxial mechanical testing; C.-H.L., Y.W., C.J.R., D.W.L. carried out the mechanical data and statistical analyses; K.-M.F., C.J.R., D.W.L., R.C.C. carried out the histology and image analyses; C.J.R., D.W.L. drafted the manuscript; C.-H.L., G.A.H., Y.W., A.M., H.M.B. critically revised the manuscript. All authors gave final approval for publication and agree to be held accountable for the work performed therein.

Competing interests. The authors of this paper have no financial or personal relationships with other people or organizations that could inappropriately influence (bias) our work.

Funding. Support from the American Heart Association Scientist Development Grant (SDG) Award (16SDG27760143) is gratefully acknowledged. C.-H.L. was in part supported by the institutional start-up funds from the School of Aerospace and Mechanical Engineering (AME) and the research funding through the Faculty Investment Program from the Research Council at the University of Oklahoma (OU). J.R., C.J.R. and D.W.L. were supported by the Mentored Research Fellowship (MRF) from the Office of Undergraduate Research (OUR) at OU.

References

1. Sacks MS, Yoganathan AP. 2007 Heart valve function: a biomechanical perspective. *Philos. Trans. R. Soc. Lond. B Biol. Sci* **362**, 1369–1391. (doi:10.1098/rstb.2007.2122)
2. Lee C-H, Carruthers CA, Ayoub S, Gorman RC, Gorman JH, Sacks MS. 2015 Quantification and simulation of layer-specific mitral valve interstitial cells deformation under physiological loading. *J. Theor. Biol.* **373**, 26–39. (doi:10.1016/j.jtbi.2015.03.004)
3. Sacks MS, David Merryman W, Schmidt DE. 2009 On the biomechanics of heart valve function. *J. Biomech.* **42**, 1804–1824. (doi:10.1016/j.jbiomech.2009.05.015)
4. Vesely I, Noseworthy R. 1992 Micromechanics of the fibrosa and the ventricularis in aortic valve leaflets. *J. Biomech.* **25**, 101–113. (doi:10.1016/0021-9290(92)90249-Z)
5. Vesely I. 1998 The role of elastin in aortic valve mechanics. *J. Biomech.* **31**, 115–123. (doi:10.1016/S0021-9290(97)00122-X)
6. Scott MJ, Vesely I. 1996 Morphology of porcine aortic valve cusp elastin. *J. Heart. Valve Dis.* **5**, 464–471.

7. Kunzelman KS, Cochran RP, Murphree SS, Ring WS, Verrier ED, Eberhart RC. 1993 Differential collagen distribution in the mitral valve and its influence on biomechanical behaviour. *J. Heart. Valve Dis.* **2**, 236–244.
8. Tseng H, Grande-Allen KJ. 2011 Elastic fibers in the aortic valve spongiosa: a fresh perspective on its structure and role in overall tissue function. *Acta Biomater.* **7**, 2101–2108. (doi:10.1016/j.actbio.2011.01.022)
9. Rothenburger M, Völker W, Vischer P, Glasmacher B, Scheld HH, Deiwick M. 2002 Ultrastructure of proteoglycans in tissue-engineered cardiovascular structures. *Tissue Eng.* **8**, 1049–1056. (doi:10.1089/107632702320934146)
10. Simionescu DT, Lovekamp JJ, Vyavahare NR. 2003 Degeneration of bioprosthetic heart valve cusp and wall tissues is initiated during tissue preparation: an ultrastructural study. *J. Heart. Valve Dis.* **12**, 226–234.
11. Grande-Allen KJ, Calabro A, Gupta V, Wight TN, Hascall VC, Vesely I. 2004 Glycosaminoglycans and proteoglycans in normal mitral valve leaflets and chordae: association with regions of tensile and compressive loading. *Glycobiology* **14**, 621–633. (doi:10.1093/glycob/cwh076)
12. Sacks MS, David Merryman W, Schmidt DE. 2009 On the biomechanics of heart valve function. *J. Biomech.* **42**, 1804–1824. (doi:10.1016/j.jbiomech.2009.05.015)
13. Schoen F. 2008 Evolving concepts of cardiac valve dynamics: the continuum of development, functional structure, pathobiology, and tissue engineering. *Circulation* **118**, 1864–1880. (doi:10.1161/CIRCULATIONAHA.108.805911)
14. Lee C-H, Carruthers CA, Ayoub S, Gorman RC, Gorman III JH, Sacks MS. 2015 Quantification and simulation of layer-specific mitral valve interstitial cells deformation under physiological loading. *J. Theor. Biol.* **373**, 26–39. (doi:10.1016/j.jtbi.2015.03.004)
15. Zhang W, Ayoub S, Liao J, Sacks MS. 2016 A meso-scale layer-specific structural constitutive model of the mitral heart valve leaflets. *Acta Biomater.* **32**, 238–255. (doi:10.1016/j.actbio.2015.12.001)
16. Talman EA, Boughner DR. 1995 Glutaraldehyde fixation alters the internal shear properties of porcine aortic heart valve tissue. *Ann. Thorac. Surg.* **60**, S369-S373. (doi:10.1016/0003-4975(95)00250-O)
17. Vyavahare N, Ogle M, Schoen FJ, Zand R, Gloeckner DC, Sacks M, Levy RJ. 1999 Mechanisms of bioprosthetic heart valve failure: fatigue causes collagen denaturation and glycosaminoglycan loss. *J. Biomed. Mater. Res.* **46**, 44–50. (doi:10.1002/(SICI)1097-4636(199907)46:1%3C44::AID-JBM5%3E3.0.CO;2-D)
18. Boorman RS, Thornton GM, Shrive NG, Frank CB. 2002 Ligament grafts become more susceptible to creep within days after surgery: evidence for early enzymatic degradation of a ligament graft in a rabbit model. *Acta Orthop. Scand.* **73**, 568–574. (doi:10.1080/000164702321022866)
19. Thornton GM, Shrive NG, Frank CB. 2002 Ligament creep recruits fibres at low stresses and can lead to modulus-reducing fibre damage at higher creep stresses: a study in rabbit medial collateral ligament model. *J. Orth. Res.* **20**, 967–974. (doi:10.1016/S0736-0266(02)00028-1)
20. Ali AF, Taha MMR, Thornton GM, Shrive NG, Frank CB. 2005 Biomechanical study using fuzzy systems to quantify collagen fiber recruitment and predict creep of the rabbit medial collateral ligament. *J. Biomech. Eng.* **127**, 484–493. (doi:10.1115/1.1894372)
21. Eckert CE, Fan R, Mikulis B, Barron M, Carruthers CA, Friebe VM, Vyavahare NR, Sacks MS. 2013 On the biomechanical role of glycosaminoglycans in the aortic heart valve leaflet. *Acta Biomater.* **9**, 4653–4660. (doi:10.1016/j.actbio.2012.09.031)
22. Azeloglu EU, Albro MB, Thimmappa VA, Ateshian GA, Costa KD. 2008 Heterogeneous transmural proteoglycan distribution provides a mechanism for regulating residual stresses in the aorta. *Am. J. Physiol. Heart Circ. Physiol.* **294**, H1197-H1205. (doi:10.1152/ajpheart.01027.2007)
23. Humphrey JD. 2013 Possible mechanical roles of glycosaminoglycans in thoracic aortic dissection and associations with dysregulated transforming growth factor-β. *J. Vasc. Res.* **50**, 1–10. (doi:10.1159/000342436)
24. Grashow JS, Yoganathan AP, Sacks MS. 2006 Biaixal stress–stretch behavior of the mitral valve anterior leaflet at physiologic strain rates. *Ann. Biomed. Eng.* **34**, 315–325. (doi:10.1007/s10439-005-9027-y)
25. Huang H-YS, Balhouse BN, Huang S. 2012 Application of simple biomechanical and biochemical tests to heart valve leaflets: implications for heart valve characterization and tissue engineering. *Proc. Inst. Mech. Eng. H* **226**, 868–876. (doi:10.1177%2F0954411912455004)
26. Jett S, Laurence D, Kunkel R, Babu AR, Kramer K, Baumwart R, Towner R, Wu Y, Lee C-H. 2018 Biaxial mechanical data of porcine atrioventricular valve leaflets. *Data Brief* **21**, 358–363. (doi:10.1016/j.dib.2018.09.073)
27. Khoiy KA, Amini R. 2016 On the biaxial mechanical response of porcine tricuspid valve leaflets. *J. Biomech. Eng.* **138**, 104504–104506. (doi:10.1115/1.4034426)
28. Pokutta-Paskaleva A, Sulejmani F, DelRocini M, Sun W. 2019 Comparative mechanical, morphological, and microstructural characterization of porcine mitral and tricuspid leaflets and chordae tendineae. *Acta Biomater.* **85**, 241–252. (doi:10.1016/j.actbio.2018.12.029)
29. Stella JA, Sacks MS. 2007 On the biaxial mechanical properties of the layers of the aortic valve leaflet. *J. Biomech. Eng.* **129**, 757–766. (doi:10.1115/1.2768111)
30. Ross C, Laurence D, Wu Y, Lee C-H. 2019 Biaxial mechanical characterizations of atrioventricular heart valves. *J. Vis. Exp.* **146**, e59170. (doi:10.3791/59170)
31. Weiler M, Yap CH, Balachandran K, Padala M, Yoganathan AP. 2011 Regional analysis of dynamic deformation characteristics of native aortic valve leaflets. *J. Biomech.* **44**, 1459–1465. (doi:10.1016/j.jbiomech.2011.03.017)
32. Chen L, McCulloch AD, May-Newman K. 2004 Nonhomogeneous deformation in the anterior leaflet of the mitral valve. *Ann. Biomed. Eng.* **32**, 1599–1606. (doi:10.1007/s10439-004-7813-6)
33. Laurence D *et al.* 2019 An investigation of regional variations in the biaxial mechanical properties and stress relaxation behaviors of porcine atrioventricular heart valve leaflets. *J. Biomech.* **83**, 16–27. (doi:10.1016/j.jbiomech.2018.11.015)
34. Mow VC, Mak AF, Lai WM, Rosenberg LC, Tang L-H. 1984 Viscoelastic properties of proteoglycan subunits and aggregates in varying solution concentrations. *J. Biomech.* **17**, 325–338. (doi:10.1016/0021-9290(84)90027-7)
35. Ratcliffe A, Mow VC. 1996 Articular cartilage. *Extracellular matrix* **1**, 234–302.
36. Zhu W, Iatridis JC, Hlibczuk V, Ratcliffe A, Mow VC. 1996 Determination of collagen–proteoglycan interactions *in vitro*. *J. Biomech.* **29**, 773–783. (doi:10.1016/0021-9290(95)00136-0)
37. Borghi AH, New SE, Chester AH, Taylor PM, Yacoub MH. 2012 Time-dependent mechanical properties of aortic valve cusps: effect of glycosaminoglycan depletion. *Acta Biomater.* **9**, 4645–4652. (doi:10.1016/j.actbio.2012.09.001)
38. Grashow JS, Sacks MS, Liao J, Yoganathan AP. 2006 Planar biaxial creep and stress relaxation of the mitral valve anterior leaflet. *Ann. Biomed. Eng.* **34**, 1509–1518. (doi:10.1007/s10439-006-9183-8)
39. Jett S, Laurence D, Kunkel R, Babu AR, Kramer K, Baumwart R, Towner R, Wu Y, Lee C-H. 2018 An investigation of the anisotropic mechanical properties and anatomical structure of porcine atrioventricular heart valves. *J. Mech. Behav. Biomed. Mater.* **87**, 155–171. (doi:10.1016/j.jmbbm.2018.07.024)
40. Lee C-H, Amini R, Gorman RC, Gorman 3rd JH, Sacks MS. 2014 An inverse modeling approach for stress estimation in mitral valve anterior leaflet valvuloplasty for *in-vivo* valvular biomaterial assessment. *J. Biomech.* **47**, 2055–2063. (doi:10.1016/j.jbiomech.2013.10.058)
41. Anssari-Benam A Tseng, Y-T, Holzapfel GA, Bucchi A. 2019 Rate-dependency of the mechanical behaviour of semilunar heart valves under biaxial deformation. *Acta Biomater.* **88**, 120–130. (doi:10.1016/j.actbio.2019.02.008)
42. Lovekamp JJ, Simionescu DT, Mercuri JJ, Zubiate B, Sacks MS, Vyavahare NR. 2006 Stability and function of glycosaminoglycans in porcine bioprosthetic heart valves. *Biomaterials* **27**, 1507–1518. (doi:10.1016/j.biomaterials.2005.08.003)
43. Shah SR, Vyavahare NR. 2008 The effect of glycosaminoglycan stabilization on tissue buckling in bioprosthetic heart valves. *Biomaterials* **29**, 1645–1653. (doi:10.1016/j.biomaterials.2007.12.009)
44. Ayoub S, Tsai KC, Khalighi AH, Sacks MS. 2018 The three-dimensional microenvironment of the mitral

valve: insights into the effects of physiological loads. *Cell. Mol. Bioeng.* **11**, 291–306. (doi:10.1007/s12195-018-0529-8)

45. Lee C-H, Zhang W, Feaver K, Gorman RC, Gorman 3rd JH, Sacks MS. 2017 On the *in vivo* function of the mitral heart valve leaflet: insights into tissue–interstitial cell biomechanical coupling. *Biomech. Model. Mechanobiol.* **16**, 1613–1632. (doi:10.1007/s10237-017-0908-4)
46. Foutz TL, Stone EA, Abrams CF. 1992 Effects of freezing on mechanical properties of rat skin. *Am. J. Vet. Res.* **53**, 788–792.
47. Stemper BD, Yoganandan N, Stineman MR, Gennarelli TA, Baisden JL, Pintar FA. 2007 Mechanics of fresh, refrigerated, and frozen arterial tissue. *J. Surg. Res.* **139**, 236–242. (doi:10.1016/j.jss.2006.09.001)
48. Ruifrok AC, Johnston DA. 2001 Quantification of histochemical staining by color deconvolution. *Anal. Quant. Cytol. Histol.* **23**, 291–299.
49. Pierlot CM, Moeller AD, Lee JM, Wells SM. 2015 Biaxial creep resistance and structural remodeling of the aortic and mitral valves in pregnancy. *Ann. Biomed. Eng.* **43**, 1772–1785. (doi:10.1007/s10439-014-1230-2)
50. Reddy JN. 2013 *An introduction to continuum mechanics*. Cambridge, UK: Cambridge University Press.
51. Tadmor EB, Miller RE, Elliott RS. 2012 *Continuum mechanics and thermodynamics: from fundamental concepts to governing equations*. Cambridge, UK: Cambridge University Press.
52. Sacks MS, Schoen FJ, Mayer Jr JE. 2009 Bioengineering challenges for heart valve tissue engineering. *Annu. Rev. Biomed. Eng.* **11**, 289–313. (doi:10.1146/annurev-bioeng-061008-124903)
53. Chiang YP, Chikwe J, Moskowitz AJ, Itagaki S, Adams DH, Egorova NN. 2014 Survival and long-term outcomes following bioprosthetic vs mechanical aortic valve replacement in patients aged 50 to 69 years. *JAMA* **312**, 1323–1329. (doi:10.1001/jama.2014.12679)
54. Hammermeister K, Sethi GK, Henderson WG, Grover FL, Oprian C, Rahimtoola SH. 2000 Outcomes 15 years after valve replacement with a mechanical versus a bioprosthetic valve: final report of the Veterans Affairs randomized trial. *J. Am. Coll. Cardiol.* **36**, 1152–1158. (doi:10.1016/S0735-1097(00)00834-2)
55. Schoen FJ. 2001 Pathology of heart valve substitution with mechanical and tissue prostheses. *Cardiovasc. Pathol.* **3**, 629–677.
56. Murata K. 1981 Acidic glycosaminoglycans in human heart valves. *J. Mol. Cell. Cardiol.* **13**, 281–292. (doi:10.1016/0022-2828(81)90316-3)
57. Sacks MS, Yoganathan AP. 2007 Heart valve function: a biomechanical perspective. *Phil. Trans. R. Soc. B* **362**, 1369–1391. (doi:10.1098/rstb.2007.2122)
58. Goth W, Potter S, Allen ACB, Zoldan J, Sacks MS, Tunnell JW. 2019 Non-destructive reflectance mapping of collagen fiber alignment in heart valve leaflets. *Ann. Biomed. Eng.* **47**, 1250–1264. (doi:10.1007/s10439-019-02233-0)
59. Cacho F, Elbischger PJ, Rodriguez JF, Doblaré M, Holzapfel GA. 2007 A constitutive model for fibrous tissues considering collagen fiber crimp. *Int. J. Non-Linear Mech.* **42**, 391–402. (doi:10.1016/j.ijnonlinmec.2007.02.002)
60. Kroon M, Holzapfel GA. 2008 A new constitutive model for multi-layered collagenous tissues. *J. Biomech.* **41**, 2766–2771. (doi:10.1016/j.jbiomech.2008.05.033)
61. Lee C-H, Rabbah J-P, Yoganathan AP, Gorman RC, Gorman III JH, Sacks MS. 2015 On the effects of leaflet microstructure and constitutive model on the closing behavior of the mitral valve. *Biomech. Model. Mechanobiol.* **14**, 1281–1302. (doi:10.1007/s10237-015-0674-0)
62. Padala M. 2018 Patient-specific computational biomechanical modeling to guide mitral valve repair strategy: practicality and value? *J. Thorac. Cardiovasc. Surg.* **155**, 606–607. (doi:10.1016/j.jtcvs.2017.09.132)
63. Sacks MS. 2003 Incorporation of experimentally-derived fiber orientation into a structural constitutive model for planar collagenous tissues. *J. Biomech. Eng.* **125**, 280–287. (doi:10.1115/1.1544508)
64. Stevanella M, Maffessanti F, Conti CA, Votta E, Arnoldi A, Lombardi M, Parodi O, Caiani EG, Redaelli A. 2011 Mitral valve patient-specific finite element modeling from cardiac MRI: application to an annuloplasty procedure. *Cardiovasc. Eng. Technol.* **2**, 66–76. (doi:10.1007/s13239-010-0032-4)
65. Holzapfel GA, Niestrawska JA, Ogden RW, Reinisch AJ, Schriefl AJ. 2015 Modelling non-symmetric collagen fibre dispersion in arterial walls. *J. R Soc. Interface* **12**, 20150188. (doi:10.1098/rsif.2015.0188)
66. Prot V, Skallerud B, Sommer G, Holzapfel GA. 2010 On modelling and analysis of healthy and pathological human mitral valves: two case studies. *J. Mech. Behav. Biomed. Mater.* **3**, 167–177. (doi:10.1016/j.jmbbm.2009.05.004)
67. Holzapfel GA, Ogden RW. 2010 Constitutive modelling of arteries. *Proc. R. Soc. London, Ser. A* **466**, 1551–1597. (doi:10.1098/rspa.2010.0058)
68. Rego BV, Wells SM, Lee C-H, Sacks MS. 2016 Mitral valve leaflet remodelling during pregnancy: Insights into cell-mediated recovery of tissue homeostasis. *J. R Soc. Interface* **13**, 20160709. (doi:10.1098/rsif.2016.0709)
69. Ambrosi D *et al.* 2011 Perspectives on biological growth and remodeling. *J. Mech. Phys. Solids* **59**, 863–883. (doi:10.1016/j.jmps.2010.12.011)
70. Humphrey JD, Rajagopal KR. 2002 A constrained mixture model for growth and remodeling of soft tissues. *M3AS* **12**, 407–430. (doi:10.1142/S0218202502001714)
71. Ross C *et al.* 2019 Data from: 'An investigation of the glycosaminoglycan contribution to biaxial mechanical behaviors of porcine atrioventricular heart valve leaflets'. Figshare Digital Repository. (doi:10.6084/m9.figshare.8179556)